Bulletin of Geophysics and Oceanography Vol. XX, n. X, pp. XXX-XXX; Xxxxx 20xx
DOI 10.4430/bgo00503

Facies classification using the convolutional neural network (CNN) algorithm in an offshore oilfield, SW of Iran

M.H. Soleimani, M.A. Riahi and M. Rahimi

Institute of Geophysics, University of Tehran, Tehran, Iran

(Received: 20 December 2024; accepted: 12 August 2025; published online: 30 September 2025)

ABSTRACT Accurate lithofacies classification is essential for effective reservoir characterisation and hydrocarbon development. This study presents a lightweight one-dimensional convolutional neural network (1D-CNN) for automated facies classification using well-log data from two offshore wells in south-western Iran. Four petrophysical logs, gamma ray, resistivity, sonic transit time, and bulk density served as input features to distinguish calcite, dolomite, and anhydrite facies. Five optimisation algorithms (Adagrad, Adadelta, Adam, Adamax, and stochastic gradient descent) were evaluated based on classification accuracy, convergence behaviour, and computational efficiency. The CNN architecture incorporates batch normalisation, dropout regularisation, and fine-tuned hyperparameters to ensure stable learning under limited data conditions. Results show that adaptive optimisers, especially Adam and Adamax, outperformed others. Adam achieved the highest accuracy (95.7%), while Adamax offered a better balance between accuracy and training efficiency. In contrast, Adadelta showed the poorest performance. Despite class imbalance and the absence of core data, the Adamax-optimised model achieved strong F1-scores across all facies. This study demonstrates the feasibility of optimised 1D-CNNs for lithofacies classification in data, and resource, constrained environments and highlights the importance of optimiser choice. Future work should include more diverse geological datasets and integrate core or seismic data for improved validation and broader applicability.

Key words: lithofacies classification, convolutional neural network, hydrocarbon exploration, machine learning.

1. Introduction

Accurate characterisation of subsurface formations is critical for optimising hydrocarbon exploration and reservoir development. Understanding lithofacies distribution enables geoscientists to interpret depositional environments, assess reservoir quality, and enhance recovery strategies. Lithofacies, which describe the physical and spatial characteristics of depositional units, are essential for guiding well placement and improving hydrocarbon extraction (Al-Mudhafar *et al.*, 2022). Robust reservoir characterisation also requires accounting for structural heterogeneities, lithological variability, and fracture networks (Milad and Slatt, 2018).

Given the importance of precise lithofacies identification in geological modelling, numerous automated and data-driven methods have emerged to support objective subsurface interpretation

and reduce expert bias (Chai *et al*., 2009). Traditional techniques such as manual interpretation of well logs, core samples, and borehole images remain widely used but are limited by subjectivity, time demands, and reliance on expert judgment (Alzubaidi *et al*., 2021). These constraints have led to the development of automated classification methods based on petrophysical logs, core data, and borehole imagery (Basu *et al.*, 2002).

With advances in computational intelligence, machine learning (ML) has emerged as a promising alternative, offering improved efficiency and reduced bias (Ceci *et al*., 2017). A variety of ML algorithms have been applied to lithofacies classification, including support vector machines and k-nearest neighbours (Cover and Hart, 1967; Boser *et al*., 1992; Alexsandro *et al*., 2017; Prabowo *et al*., 2023). While effective in simpler geological settings, these models often struggle in heterogeneous carbonate reservoirs due to their limited ability to capture non-linear and complex patterns (Dubois *et al*., 2007). Boosting techniques have been introduced to improve performance, yet challenges persist in addressing geological heterogeneity and data non-stationarity.

Recent developments highlight the strong potential of deep learning approaches, particularly convolutional neural networks (CNNs), for subsurface classification. CNNs can extract hierarchical spatial features from input data, enabling accurate lithofacies prediction even in the absence of core samples (Hall *et al*., 1996). One-dimensional CNNs (1D-CNNs) are particularly well-suited for processing well-log data, capturing fine-scale lithological patterns (Hall, 2016; Imamordiev and Sukhosta, 2019). Prior studies have also demonstrated CNN effectiveness in analysing core computerised tomography scans (Newberry *et al*., 2004; Chawshin *et al*., 2021) and recognising geological textures across various depositional settings (Li *et al*., 2015).

Despite these advancements, key challenges remain. Many CNN-based studies require substantial computational resources, limiting their field applicability. Issues such as model convergence, stability, and overfitting, particularly under data-limited conditions, are frequently encountered, and few works offer systematic solutions. Techniques such as batch normalisation have been proposed to improve training efficiency and reduce internal covariate shift (Ioffe and Szegedy, 2015). However, the role of optimisation algorithms in training performance and generalisation remains underexplored, as many studies employ a single optimiser without comparative evaluation.

Recent research has advocated for combining adaptive and non-adaptive optimisers to enhance training. Adaptive methods such as Adagrad, Adadelta, Adam, and Adamax adjust learning rates dynamically, promoting faster convergence and improved generalisation (Hastie *et al*., 2009; Zeiler, 2012; Kingma and Ba, 2014), while non-adaptive methods like stochastic gradient descent (SGD) offer stability in certain geological applications (Duchi *et al.*, 2011). Yet, comparative analyses of these optimisers within lithofacies classification remain scarce.

Alternative approaches such as random forests, fuzzy logic, naïve Bayes classifiers, and discriminant analysis have also been applied to geological datasets with mixed success (Saggaf and Nebrija, 2003; Li and Anderson-Sprecher, 2006). Techniques like resistivity imaging and prestack seismic inversion have further contributed to facies prediction in complex reservoirs (Linek *et al*., 2007; Moghanloo *et al*., 2018; Rahimi and Riahi, 2022). However, the integration of CNN architectures with rigorous optimiser evaluation, especially in data-scarce or computationally constrained settings, remains a largely unexplored research niche.

In this study, we present and evaluate a lightweight CNN architecture optimised for accurate and efficient lithofacies classification. By conducting a comprehensive comparison of adaptive (Adagrad, Adadelta, Adam, Adamax) and non-adaptive (SGD) optimisers, we assess their impact on convergence, generalisation, and classification accuracy. Addressing key gaps in current

literature, this work contributes to the development of scalable, robust deep learning frameworks for lithofacies prediction under realistic operational constraints.

2. Geological setting

This study investigates a hydrocarbon-bearing offshore field located in the south-western region of Iran. The area encompasses several major stratigraphic units, including the Kangan, Dalan, Asmari, Pabdeh, and Gachsaran formations, which collectively exhibit a broad range of lithologies such as limestone, dolomite, evaporites, and shale. Structurally, the field is situated along the north-eastern margin of the Zagros Fold – Thrust Belt and is superimposed on the Qatar Arch (Fig. 1), a prominent NW-SE-trending basement high that marks the boundary between the Zagros foreland basin and the Qatar-Fars Arch. The absence of the Cambrian Hormuz Salt in this region has contributed to the relative tectonic stability of the arch and played a significant role in shaping the area's structural evolution (Perotti *et al*., 2011). Ongoing convergence between the Arabian and Eurasian plates has resulted in considerable sediment accumulation in the Zagros basin, whereas the Qatar Arch has undergone only limited subsidence, maintaining its elevated structural character.

Hydrocarbon accumulations in this field are primarily associated with carbonate reservoirs from the Upper Permian to Lower Triassic, while Silurian-aged shales act as the main source rocks (Esrafili-Dizaji *et al*., 2013). The geological map presented in Fig. 1, compiled using data from Pollastro *et al*. (1999) and Geographic Information System (GIS) layers from GISGeography (2025), illustrates the regional tectonic framework, major oil and gas fields, and prevailing structural trends across south-western Iran. This map also highlights the lithostratigraphic

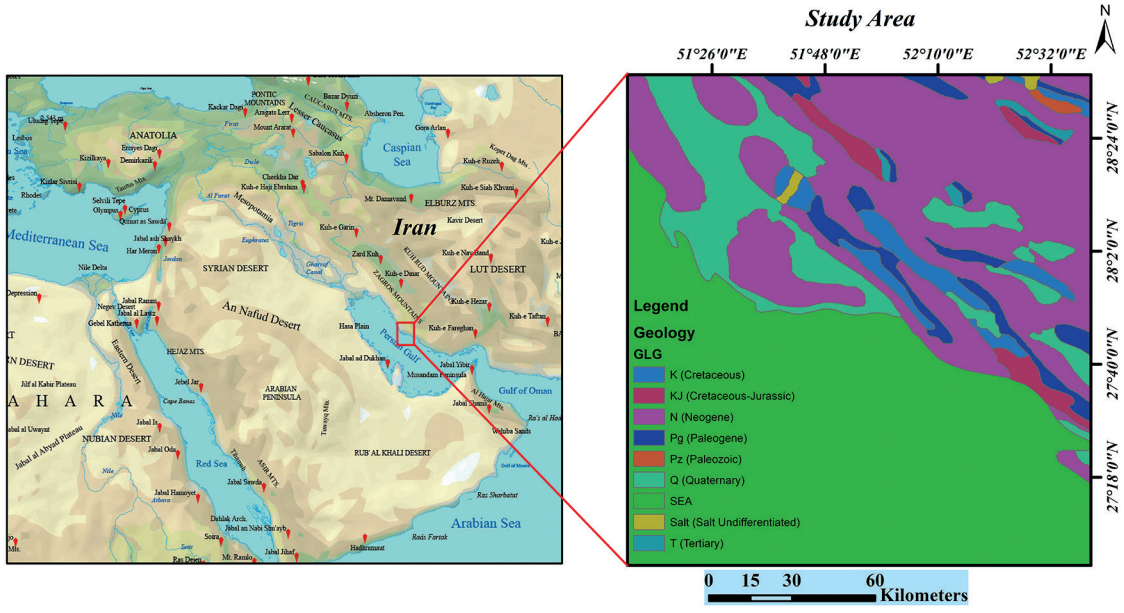

Fig. 1 - Geological map of south-western Iran highlighting the studied offshore hydrocarbon field (outlined in red). The map illustrates major tectonic zones, hydrocarbon fields, and stratigraphic units ranging from the Precambrian to the Cenozoic, including extensive Mesozoic-Tertiary carbonate formations and Miocene evaporites.

complexity of the region, which includes sedimentary successions ranging from the Precambrian to the Cenozoic. Notably, widespread carbonate and clastic formations of Mesozoic and Tertiary age serve as prolific reservoir rocks within much of the Zagros basin. Additionally, the Miocene-aged evaporitic Gachsaran Formation, which is extensively mapped throughout the area, functions as a major regional seal, promoting the effective entrapment of hydrocarbons both above and below its interval.

The red polygon in Fig. 1 delineates the study area, where two exploratory wells were drilled and utilised in this research. These wells penetrate a representative stratigraphic column of the basin, encompassing key carbonate reservoirs within the Kangan and Dalan formations and the overlying evaporitic units of the Dashtak and Gachsaran formations. This structural and stratigraphic context provides a robust framework for testing ML models aimed at automated lithofacies classification using well-log data.

The field was discovered in 1990 by the National Iranian Oil Company as part of a broad hydrocarbon exploration campaign in the Persian Gulf. Since its discovery, it has evolved into one of Iran's largest gas accumulations and remains a cornerstone of the country's offshore energy strategy.

Fig. 2 presents a generalised stratigraphic column of the south-western offshore region, summarising the key lithostratigraphic units encountered in the study area. The sequence spans from the Upper Permian to the Miocene and includes, from base to top, the Dalan, Kangan, Dashtak, Asmari, Pabdeh, and Gachsaran formations. Within the Permian-Triassic interval, the Kangan and upper Dalan formations are subdivided into four informal units, designated K1 through K4, based on vertical lithological variations. These consist of alternating carbonate and evaporite layers and represent the principal stratigraphic intervals analysed in this study. The overlying Dashtak Formation is mainly composed of shale and anhydrite, while the upper succession includes the Asmari, Pabdeh, and Gachsaran formations, which reflect continued sedimentation into the Cenozoic. This stratigraphic column provides a regional context for understanding the vertical distribution of the lithological units in the studied wells, with intervals corresponding to the facies classification conducted via the 1D-CNN model applied in this research.

3. Materials and methods

This study presents a comprehensive methodology for lithofacies classification using a lightweight 1D-CNN trained on well-log data acquired from an offshore hydrocarbon field in south-western Iran. The workflow comprises dataset characterisation, rigorous preprocessing, model architecture design, hyperparameter tuning, and performance evaluation using multiple classification metrics. Each of these components is described in detail in the following sections.

3.1. Dataset

The input feature set comprises four essential petrophysical logs: bulk density (RHOB), gamma ray (GR), resistivity (RD), and sonic travel time (DT). These logs capture critical geological and petrophysical variations within the subsurface and serve as the foundation for lithofacies discrimination. Fig. 3 illustrates the vertical facies distribution across the dataset, highlighting the thickness and variability of the interpreted intervals. Fig. 4 presents detailed well-log profiles for wells A and B, respectively, including GR, DT, RHOB, and RD curves alongside corresponding

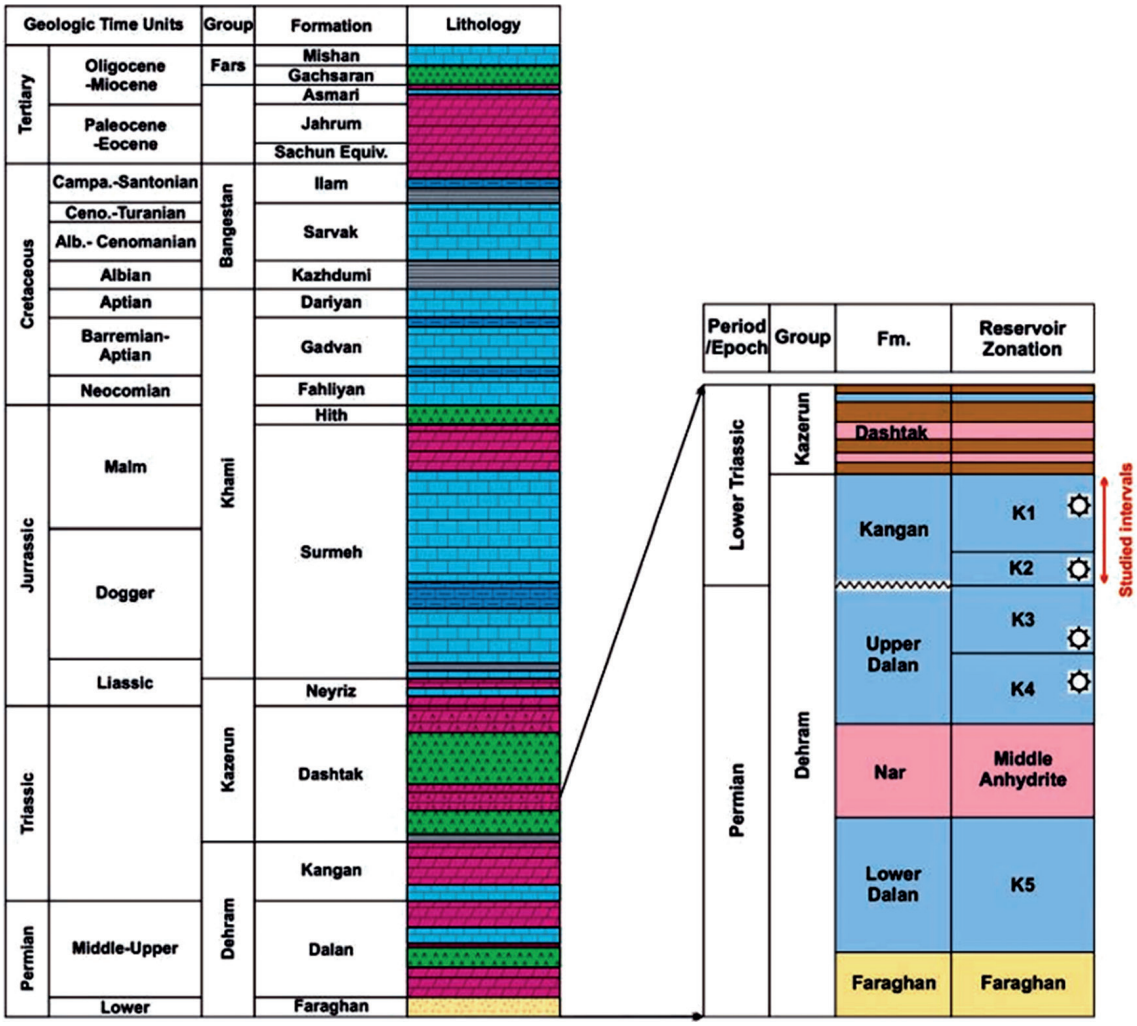

Fig. 2 - Generalised stratigraphic column of south-western Iran. The gas-producing interval is hosted within the Upper Dalan and Kangan carbonate formations. This reservoir succession is overlain by the shaley and anhydritic Dashtak Formation and subdivided into four main informal units, designated K1 through K4. The Kangan Formation (units K1 and K2) constitutes the upper part of the reservoir system in the field (Esrafili-Dizaji *et al.*, 2013).

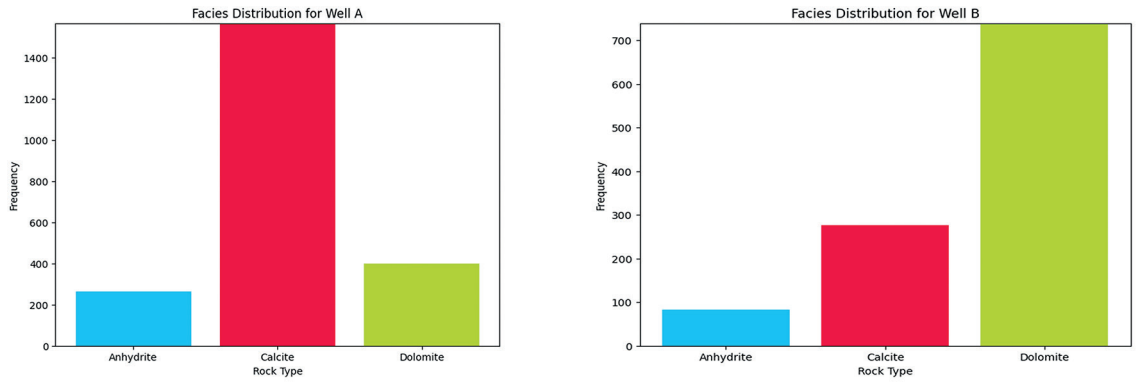

Fig. 3 - Facies distribution of wells A and B.

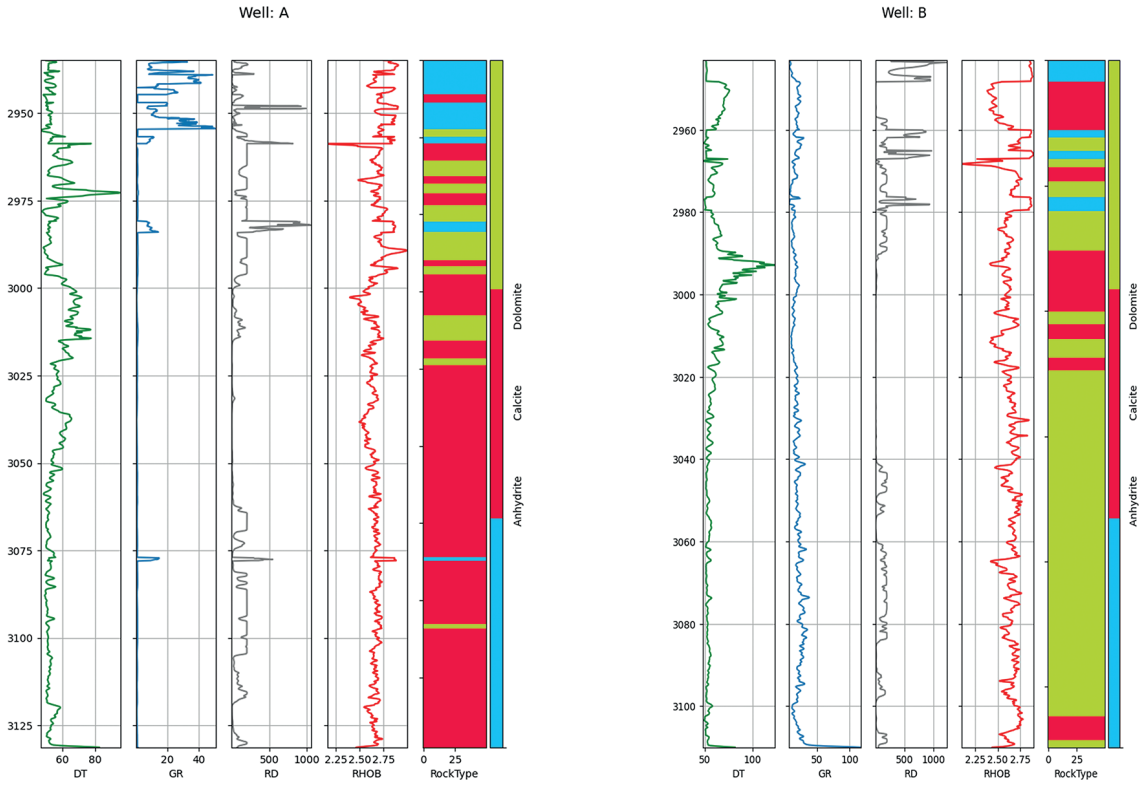

Fig. 4 - Geophysical well logs (DT, GR, RD, RHOB) and lithological interpretations for wells A and B.

lithological interpretations and facies classifications. These visualisations help to elucidate the relationships between measured rock properties and facies types, reinforcing the model's capacity to differentiate between distinct geological units.

3.1.1. Data preprocessing

Preprocessing begins with statistical characterisation of the input dataset, as summarised in Table 1. This table presents descriptive statistics for the principal well-log parameters: DT, GR, RD, depth (DEP), and RHOB. The depth range spans from 2,934.77 to 3,131.27 m. DT measurements exhibit a mean of 56.28 µs/ft, ranging from 46.64 to 123.55 µs/ft, with a standard deviation of 7.67 µs/ft. GR readings average 8.45 API units, spanning from 0.55 to 117.56 API units, and display a standard deviation of 10.09 API units. RD values vary significantly, from 0.92 to 1,235.90 Ω·m due to geological heterogeneity, with a mean of 103.94 Ω·m and a standard deviation of 136.15 Ω·m. RHOB measurements average 2.66 g/cm³, ranging from 2.10 to 2.99 g/cm³, with a standard deviation of 0.09 g/cm³, indicating relatively stable density variations across the formation. These statistical insights inform model design and provide valuable context for interpreting subsurface lithological variability.

Following this exploratory analysis, the dataset is split into training and testing subsets using a 70:30 ratio with a fixed random seed (random_state = 42) to ensure reproducibility. Facies labels are, then, transformed into one-hot encoded vectors to suit categorical classification tasks. All input features are standardised using scikit-learn StandardScaler to achieve zero mean

Table 1 - The numerical description of the dataset.

	DEP	DT	GR	RD	RHOB
Count	3324	3324	3324	3324	3324
Mean	3030.912965	56.283161	8.445974	103.941330	2.661942
std	54.187131	7.670522	10.091262	136.149687	0.094249
Min	2934.767100	46.639633	0.554627	0.924911	2.101453
25%	2984.297050	51.461474	1.187467	10.485102	2.615146
50%	3030.626250	53.460350	1.460629	60.266562	2.663260
75%	3077.108025	58.901227	16.098550	193.092327	2.703322
Max	3131.270000	123.551620	117.555191	1235.899902	2.99640

and unit variance across attributes. To accommodate the Conv1D model structure, the data is reshaped into a three-dimensional (3D) array (samples × timesteps × features), matching the expected input dimensions. This preprocessing pipeline ensures data consistency and lays a robust foundation for accurate and generalisable model training.

3.1.2. Data limitations

The dataset used in this study is derived exclusively from two exploration wells, labelled A and B, drilled within a single offshore field in south-western Iran. Although these wells sample distinct lithofacies with measurable variations in petrophysical properties, the limited dataset size restricts both geological diversity and statistical representativeness. This limitation is particularly significant in the context of subsurface heterogeneity, which varies considerably across basins and depositional environments.

A notable constraint is the absence of core samples, which limits the ability to conduct direct lithological verification and introduces a dependence on log-based facies interpretations. This reliance may lead to uncertainty in facies labelling. Moreover, the geographic restriction to a single field poses the risk of overfitting, whereby the model captures local depositional patterns that may not generalise well to other geological settings.

Table 2 presents the distribution of facies classes across the dataset, revealing substantial class imbalance: calcite (1,842 samples) dominates the dataset, followed by dolomite (1,136 samples), and anhydrite (346 samples). Such an imbalance may negatively affect model performance, especially in predicting minority classes. Fig. 5 displays a cross-plot matrix showing pairwise relationships between the primary petrophysical logs (DT, GR, RD, and RHOB), segmented by facies. Diagonal plots depict feature distributions within each facies class, while off-diagonal scatterplots illustrate inter-feature correlations. Although this visualisation confirms internal consistency within the dataset, it cannot substitute external validation sources such as core descriptions or seismic interpretation.

Table 2 - The number of each facies in the total data.

Facies type	Number of each facies
Anhydrite	346
Calcite	1842
Dolomite	1136

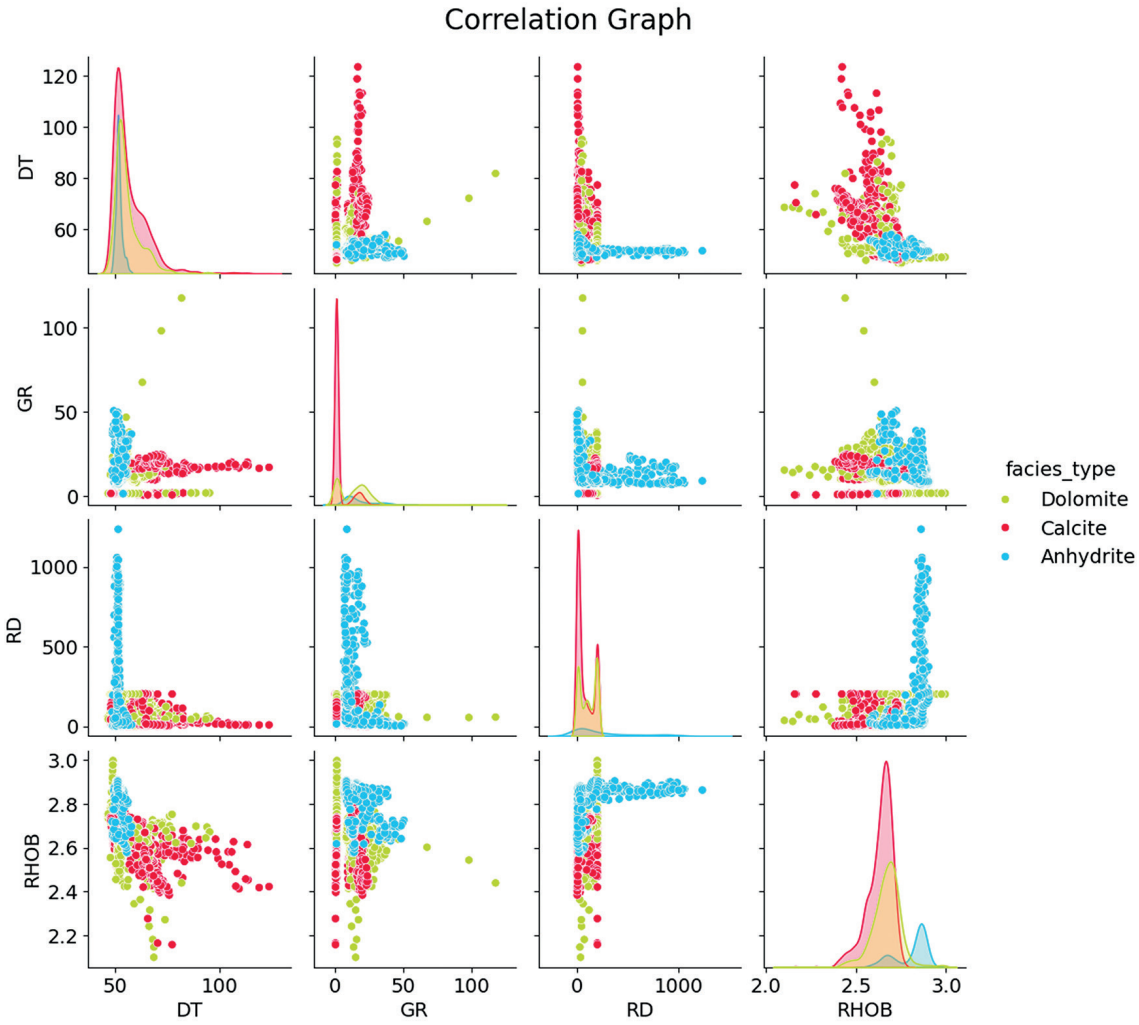

Fig. 5 - Cross-plot matrix illustrating the distribution and correlation of key well-log parameters (DT, GR, RD and RHOB) across different facies types: dolomite, calcite, and anhydrite. Diagonal histograms display the distribution of each parameter within facies classes, while off-diagonal scatter plots reveal inter-parameter relationships and clustering trends among the lithofacies.

Despite these limitations, the study implements a rigorous preprocessing workflow, deliberate model design, and a balanced training procedure to reduce overfitting and improve generalisation. Initial experimental results suggest that the model demonstrates promising robustness, although further validation is required. Future work should address current constraints by incorporating additional wells from diverse geological contexts, integrating core data for facies ground-truthing, and supplementing petrophysical logs with other data types such as borehole images or seismic attributes. These enhancements would improve model performance, reduce interpretational bias, and extend the applicability of the facies classification framework to a wider range of depositional settings.

3.2. Methodology

Fig. 6 outlines the complete methodological workflow, spanning from raw well-log data acquisition to final model evaluation. The process begins with rigorous data preparation, including cleaning, normalisation, and transformation of well-log measurements, followed by the construction and optimisation of a lightweight 1D-CNN for lithofacies classification. After model training, performance is assessed using a suite of complementary classification metrics. Each step of this workflow is described in detail below to ensure transparency and reproducibility.

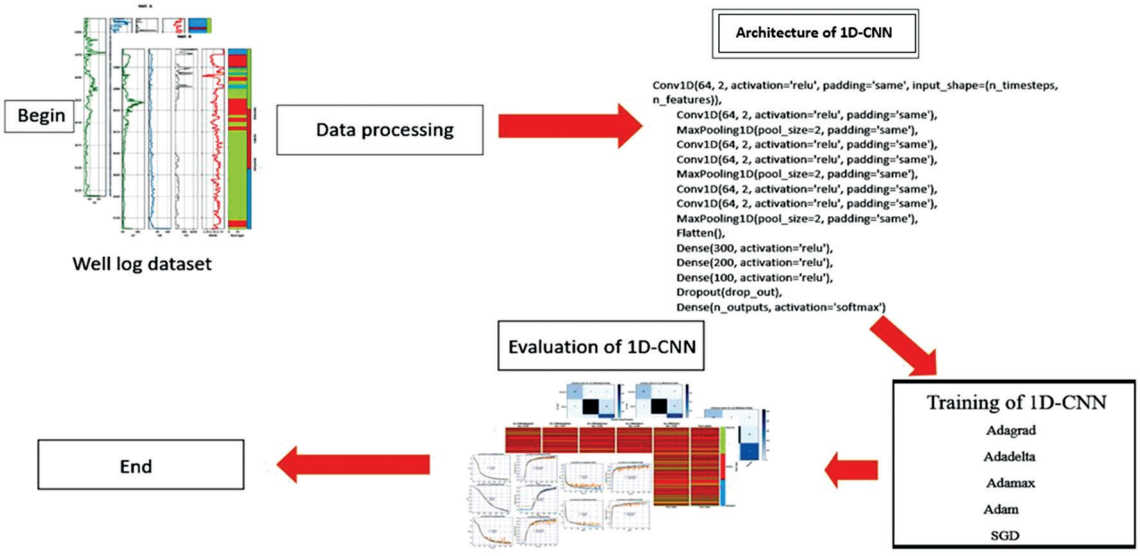

Fig. 6 - Workflow diagram illustrating the sequential steps of the study, from data acquisition and preprocessing to model training and performance evaluation.

3.2.1. Data preparation

The input dataset comprises 3,325 depth-indexed samples derived from two wells. A structured preprocessing pipeline was applied to ensure data integrity, consistency, and compatibility with the 1D-CNN architecture. Missing values in each petrophysical feature RHOB, GR, RD, and DT were imputted using the column-wise mean via scikit-learn SimpleImputer (strategy='mean'). Outliers, identified as values exceeding three standard deviations from the mean, were clipped to the 5th–95th percentile range to reduce their impact on model convergence.

All input features were, then, standardised using StandardScaler to achieve zero mean and unit variance, which is essential for improving training stability and speed. Facies labels were encoded using OneHotEncoder to accommodate multi-class classification. The dataset was subsequently reshaped into a 3D tensor (samples × timesteps × features) compatible with Conv1D input requirements and partitioned into training and testing subsets using a 70:30 split. A fixed random seed (random_state = 42) was used to ensure reproducibility and preserve class distribution across the splits.

3.2.2. CNN architecture and hyperparameter selection

The proposed 1D-CNN consists of three sequential convolutional blocks. Each block includes two Conv1D layers [64 filters, kernel size = 2, rectified linear unit (ReLU) activation, same padding], followed by a MaxPooling1D layer with a pool size of 2. The choice of a small kernel size (2) enables the model to capture abrupt transitions at lithofacies boundaries while minimising excessive smoothing. The number of filters (64) was selected via grid search from a candidate set {32, 64, 128}, balancing model expressiveness and computational efficiency.

To stabilise training and reduce internal covariate shift, batch normalisation was applied after each convolutional layer. A dropout layer with a 20% rate tuned over the range {10%, 20%, 30%} was inserted after the final pooling operation to mitigate overfitting. The output of the convolutional backbone was flattened and passed through three fully connected layers with 300, 200, and 100 neurons, respectively, each employing ReLU activation. These dimensions were empirically determined based on performance evaluations across layer sizes {100, 200, 300, 400}.

The output layer consists of a fully connected dense layer with three units and softmax activation, producing class-probability scores for anhydrite, calcite, and dolomite. Model training was performed using the Adamax optimiser at a learning rate of 0.002, selected for its stable convergence behaviour during preliminary experiments. A batch size of 64 was adopted to balance generalisation and gradient estimation. Early stopping with a patience of 15 epochs was implemented to prevent overfitting by monitoring validation loss.

The model was developed using Python in the Google Colab environment, leveraging TensorFlow, NumPy, and Pandas libraries. This configuration, coupled with grid search optimisation, ensures that the model design is both transparent and reproducible. The full network architecture is depicted in Fig. 7.

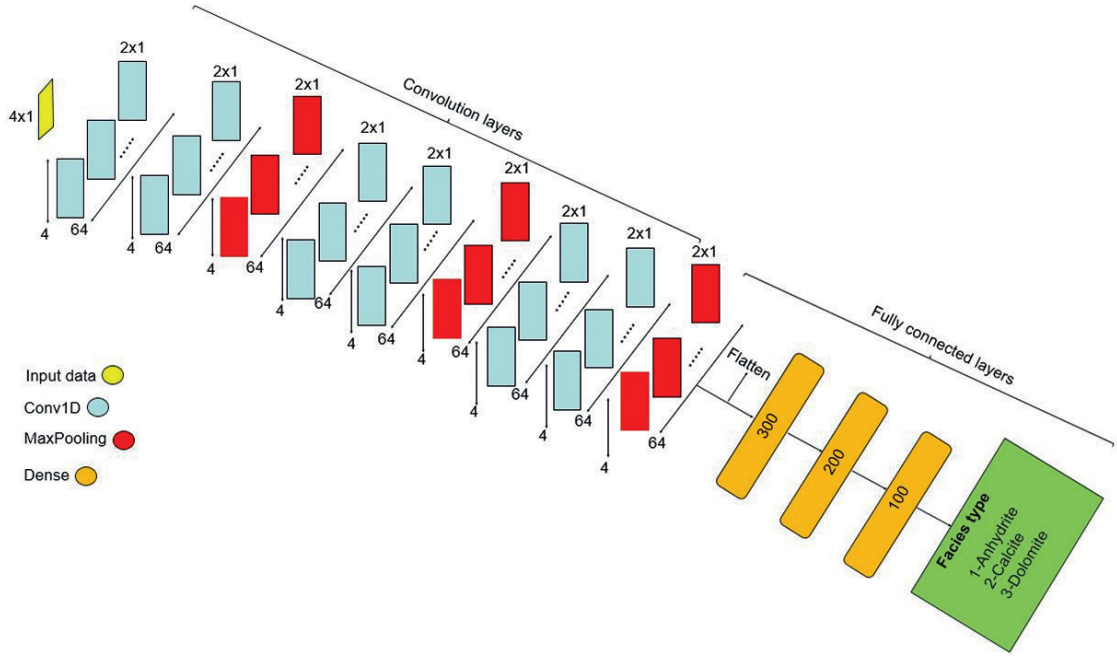

Fig. 7 - Schematic of the proposed 1D-CNN architecture for facies classification.

3.2.3. Evaluation metrics

Model performance was assessed using a comprehensive set of classification metrics. Overall categorical accuracy provides a general measure of the percentage of correctly predicted samples across all facies. However, due to class imbalance, accuracy alone may be misleading. To address this, class-specific precision, recall, and F1-score were reported.

Precision quantifies the proportion of true positives among predicted samples for each facies type, indicating susceptibility to false positives. Recall measures the proportion of actual facies correctly identified, emphasising the model's ability to detect minority classes. The F1-score, as the harmonic mean of precision and recall, provides a balanced indicator of classification quality for each facies.

In addition to these metrics, a confusion matrix was analysed to visualise patterns of misclassification, such as frequent confusion between calcite and dolomite, highlighting areas for potential refinement. By incorporating both overall and class-specific metrics, this evaluation framework offers a nuanced understanding of the model's strengths and weaknesses, guiding future improvements in both algorithmic design and geological interpretation.

4. Results

We evaluated five optimisation algorithms, Adagrad, Adadelta, Adam, Adamax, and SGD, to train efficient 1D-CNN models for lithofacies classification. Adagrad and Adadelta were initially configured with a dropout rate of 0.2, a batch size of 32, and early stopping with a patience of 15 epochs to prevent overfitting. For Adam and SGD, the dropout rate was increased to 0.5, and the batch size was set to 64, while maintaining the same early stopping configuration. Adamax was also trained with a 0.5 dropout rate and a batch size of 64. All hyperparameters were selected via grid search to achieve a practical balance between model complexity and performance, ultimately contributing to more robust classification results.

The goal of this analysis is to assess the effectiveness of these five optimisers within the context of a 1D-CNN-based facies classification task. We interpreted the results drawn from classification reports, accuracy and loss curves, and confusion matrices for both training and validation datasets. The confusion matrix is particularly useful for identifying misclassification trends, such as systematic confusion between similar lithologies.

To visual the training dynamics, we plotted model accuracy across epochs. A comparative analysis of optimiser performance, summarised in Table 3, reveals notable differences. In addition to test accuracy and loss values for the training, validation, and test datasets, Table 3 includes

Table 3 - Evaluation of the proposed model for facies classification.

Model	Training loss	Validation loss	Test loss	Validation accuracy (%)	Training accuracy (%)	Training time (seconds)	Epoch number
1D-CNN (Adagrad)	0.17	0.19	0.19	0.92%	94%	184.93	355
1D-CNN (Adadelta)	0.39	0.41	0.37	84%	84%	432.62	608
1D-CNN (Adamax)	0.08	0.13	0.18	94%	96%	111.97	128
1D-CNN (Adam)	0.04	0.19	0.19	95.7%	97.4%	72.18	155
1D-CNN (SGD)	0.16	0.18	0.18	92%	94%	130.65	142

total training time (in seconds) and the number of epochs completed. These additional metrics offer insight into the computational efficiency and convergence behaviour of each optimisation method, supporting a comprehensive evaluation of their overall effectiveness.

Tables 4 through 8 present detailed classification results for the 1D-CNN model trained with each optimiser. For every facies class, calcite, dolomite, and anhydrite, these tables report precision, recall, F1-score, and overall accuracy, offering a more nuanced view of model performance.

Table 4 - 1D_CNN (Adagrad) model classification report.

Facies type	Precision	Recall	F1-Score	Support
Anhydrite	1.00	0.99	1.00	108
Calcite	0.95	0.92	0.93	544
Dolomite	0.88	0.92	0.90	346
		Accuracy	0.93	998

Table 5 - 1D_CNN (Adadelta) model classification report.

Facies type	Precision	Recall	F1-Score	Support
Anhydrite	0.92	0.83	0.87	108
Calcite	0.91	0.89	0.90	544
Dolomite	0.79	0.84	0.81	346
		Accuracy	0.87	998

Table 6 - 1D_CNN (Adamax) model classification report.

Facies type	Precision	Recall	F1-Score	Support
Anhydrite	1.00	0.99	1.00	108
Calcite	0.98	0.92	0.95	544
Dolomite	0.88	0.97	0.93	346
		Accuracy	0.94	998

Table 7 - 1D_CNN (Adam) model classification report.

Facies type	Precision	Recall	F1-Score	Support
Anhydrite	0.99	0.99	0.99	108
Calcite	0.98	0.94	0.96	544
Dolomite	0.91	0.96	0.94	346
		Accuracy	0.95	998

Table 8 - 1D_CNN (SGD) model classification report.

Facies type	Precision	Recall	F1-Score	Support
Anhydrite	0.98	0.97	0.98	108
Calcite	0.95	0.93	0.94	544
Dolomite	0.88	0.91	0.90	346
		Accuracy	0.93	998

Fig. 8 displays the training and validation loss and accuracy curves for each optimiser. These curves reveal key differences in convergence behaviour, learning stability, and generalisation across the five optimisers. Adam and Adamax demonstrate the smoothest and most stable learning trajectories.

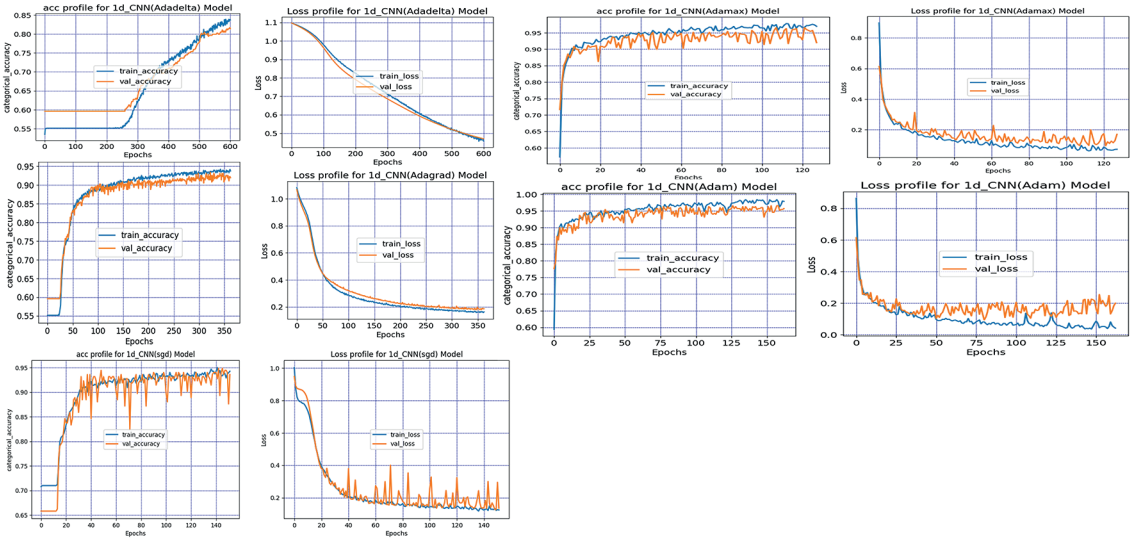

Fig. 8 - Loss function curves and facies classification accuracy for training and validation datasets for 1D-CNN (Adagrad), 1D-CNN (Adadelta), 1D-CNN (Adamax), 1D-CNN (Adam), and 1D-CNN (SGD).

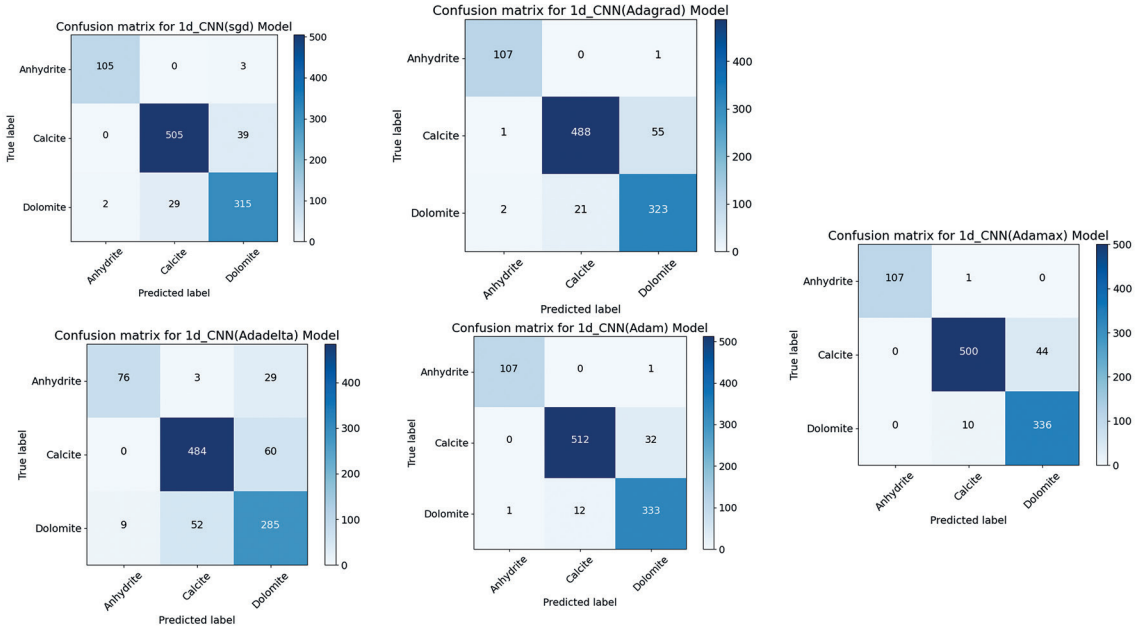

Fig. 9 - Comparison of the data confusion matrix for 5 models used in the test [1D-CNN (Adam), 1D-CNN, (Adagrad), 1D-CNN (Adadelta), 1D-CNN (Adamax), 1D-CNN (SGD)].

Fig. 9 presents the confusion matrices for all five optimisers. Adam achieved the highest classification performance, with minimal misclassifications across all facies. Adamax followed closely, also delivering strong generalisation. Adagrad and SGD showed moderate results, though both struggled with correctly classifying dolomite samples. Adadelta exhibited the weakest performance, misclassifying a large number of dolomite and anhydrite instances, indicating poor generalisation.

Finally, Fig. 10 compares the optimisers' classification results relative to true facies labels. Each plot shows the predicted versus actual class distributions, facilitating a side-by-side visual comparison of model effectiveness. Overall, Adam and Adamax emerged as the most effective optimisers for facies classification in this study.

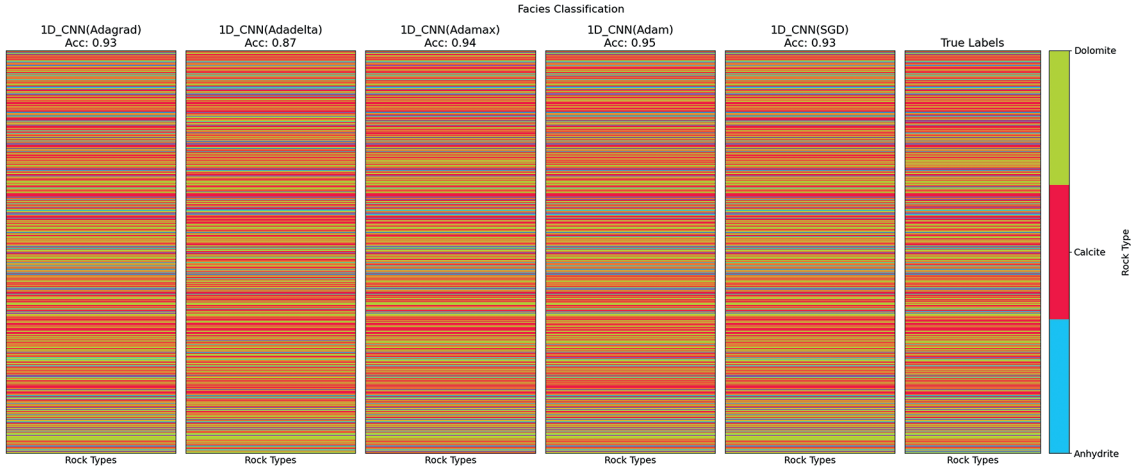

Fig. 10 - Facies classification performance comparison across different optimisation algorithms.

5. Discussion

This study presents a detailed evaluation of five optimisation algorithms, Adagrad, Adadelta, Adam, Adamax, and SGD within a 1D-CNN framework for lithofacies classification. The analysis extends beyond standard classification accuracy, incorporating additional metrics such as precision, recall, F1-score, and computational indicators (training time and number of epochs) to comprehensively assess each optimiser's performance. In this section, we synthesis and interpret these findings, compare the performance of the different optimisers, and highlight the strengths and weaknesses of each approach.

5.1. Convergence behaviour and training efficiency

Although training was permitted for up to 1,000 epochs, early stopping was employed to reduce overfitting and computational cost. As shown in Table 2, the optimisers exhibited diverse convergence profiles. Adagrad completed training in 355 epochs with a total training time of 184.93 seconds. Adadelta, the slowest to converge, required 608 epochs and 432.62 seconds. In contrast, Adamax and Adam achieved substantially faster convergence, completing training in 128 and 155 epochs, with training times of 111.97 and 72.18 seconds, respectively. Adam

demonstrated the highest computational efficiency among all optimisers, producing optimal results with the shortest training duration. SGD exhibited moderate efficiency, converging in 142 epochs over 130.65 seconds.

5.2. Underlying optimiser characteristics

Performance differences among the optimisers are primarily attributable to their intrinsic characteristics, particularly adaptive learning mechanisms, momentum, batch size, and numerical stability. Adam and Adamax, both of which employ momentum and dynamically adjust learning rates, converged faster and in a more stable manner than Adagrad and Adadelta, which lack such mechanisms. Larger batch sizes (64 for Adam, Adamax, and SGD) further contributed to smoother gradient updates and improved convergence. Adam stood out for its superior training efficiency and convergence speed, making it well-suited for applications where computational resources are limited.

5.3. Classification accuracy and model performance

The classification performance of each optimiser was evaluated through both high-level training metrics (Table 3) and facies-specific classification reports (Tables 4 to 8). Adagrad achieved a training accuracy of 94% and a validation accuracy of ~92%, with corresponding loss values of 0.17 (training), 0.19 (validation), and 0.19 (test). Adadelta performed significantly worse, converging slowly with a training accuracy of only 84% and higher loss values (training: 0.39, validation: 0.41, test: 0.37). In contrast, Adamax delivered strong results with 96% training accuracy, 94% validation accuracy, and low loss values (training: 0.08, validation: 0.13, test: 0.18).

Adam achieved the highest overall performance, converging in 155 epochs with a training time of only 72.18 seconds. It recorded a training accuracy of 97.4% and validation accuracy of 95.7%, with remarkably low loss values (training: 0.04, validation: 0.19, test: 0.19). SGD also performed well (training accuracy: 94%, validation: 92%), with balanced loss values comparable to those of Adam.

Facies-specific metrics reinforced these trends. The Adagrad-based model (Table 4) achieved perfect classification for anhydrite (precision: 1.00, recall: 0.99, F1-score: 1.00) and solid performance for calcite and dolomite, resulting in an overall accuracy of 93%. Adadelta (Table 5), however, underperformed across all classes, especially dolomite (F1-score: 0.81), with the lowest overall accuracy of 87%.

Adamax (Table 6) demonstrated near-perfect classification for anhydrite and strong results for calcite and dolomite, achieving an overall accuracy of 94%. The Adam-based model (Table 7) further improved on this, attaining near-perfect scores across all classes and the highest overall accuracy of 95%. SGD (Table 8) maintained consistent but slightly lower performance, with 93% overall accuracy.

In summary, the adaptive, momentum-based optimisers, particularly Adam and Adamax, offered superior classification accuracy, faster convergence, and greater computational efficiency than the other algorithms. Adam emerged as the best-performing optimiser overall.

5.4. Generalisation and limitations

While the results demonstrate that a compact 1D-CNN optimised with Adam or Adamax can achieve high accuracy with efficient training, several limitations must be acknowledged.

First, the dataset is derived from only two wells in the South Pars field, limiting geological diversity. Variability in depositional environments, lithology, and logging tool calibration across different reservoirs may reduce the model's generalisability. A model trained on local lithofacies distributions may not transfer effectively to other geological settings with distinct mineralogies or petrophysical signatures.

Second, facies labelling relies exclusively on well-log data, without supporting core or petrographic validation. This introduces a degree of uncertainty, particularly in intervals where log responses are ambiguous or transitional. The absence of physical samples reduces the reliability of the ground-truth facies interpretations.

Third, the dataset, although sufficient for initial model training, contains only 3,324 depth-indexed samples, which may underrepresent rare facies and subtle lithological transitions. As a result, classifier performance may be biased toward dominant classes, reducing accuracy on underrepresented lithologies.

To address these limitations and enhance the model's generalisability, future work will involve assembling a more diverse training dataset that includes well logs from multiple fields encompassing a wider range of geological environments and logging conditions. Integration of core-derived facies labels supported by petrographic and geochemical analyses will provide a stronger ground-truth foundation for model training. Advanced validation strategies, such as k-fold cross-validation and well-level hold-out testing, will be employed to assess model transferability. Additionally, synthetic data augmentation techniques such as noise injection or the generation of synthetic well logs will be explored to improve class balance and robustness against logging artifacts.

Through these enhancements, we aim to validate and extend the utility of the Adamax-driven lightweight CNN framework for reliable, efficient facies classification across a broad spectrum of geological contexts and operational environments.

6. Conclusions

This study developed a lightweight and efficient deep learning framework for lithofacies classification using well-log data from an offshore hydrocarbon field in south-western Iran. By designing an optimised 1D-CNN and systematically comparing five optimisation algorithms, Adagrad, Adadelta, Adam, Adamax, and SGD, we aimed to enhance classification accuracy, reduce computational cost, and identify the most effective training strategy for resource-constrained environments.

The results demonstrate that adaptive, momentum-based optimisers particularly Adam and Adamax, substantially improve model performance by accelerating convergence, reducing overfitting, and effectively capturing complex geological patterns. While Adam achieved the highest overall accuracy, Adamax offered the best trade-off between performance and computational efficiency, delivering high classification accuracy with the shortest training time. This makes Adamax especially suitable for real-time or operational scenarios with limited computational resources.

The streamlined 1D-CNN architecture further contributed to robust facies prediction, even in the absence of core validation data, by successfully extracting patterns solely from well-log measurements. These findings highlight the importance of combining efficient model architecture with adaptive optimisation strategies, especially Adamax, for scalable and practical subsurface facies classification.

Future research should focus on expanding the dataset to include geologically diverse fields and integrating core or seismic data to strengthen model validation. Overall, this study provides a solid foundation for broader applications of deep learning in reservoir characterisation and hydrocarbon exploration.

Acknowledgments. This research received no funding from any sector or grant. The data used and analysed in this study are available from the authors upon reasonable request; however, due to restrictions associated with proprietary well-log data, access may be subject to institutional or data-sharing agreements. Likewise, the code developed for this study, including the 1D-CNN model and optimisation algorithms, is available from the authors upon reasonable request. The authors would like to express their gratitude to the Research Council of the University of Tehran for their scientific support.

REFERENCES

Al-Mudhafar W.J., Abbas M.A. and Wood D.A.; 2022: *Performance evaluation of boosting machine learning algorithms for lithofacies classification in heterogeneous carbonate reservoirs.* Mar. Petrol. Geol., 145, 105886, doi: 10.1016/j.marpetgeo.2022.105886.

Alexsandro G.C., Carlos A.C. da P. and Geraldo G.N.; 2017: *Facies classification in well logs of the Namorado oilfield using support vector machine algorithm.* In: Proc. 15th International Congress of the Brazilian Geophysical Society & EXPOGEF, Rio de Janeiro, Brazil, pp. 1853-1858, doi: 10.1190/sbgf2017-365.

Alzubaidi F., Mostaghimi P., Swietojanski P., Clark S.R. and Armstrong R.T.; 2021: *Automated lithology classification from drill core images using convolutional neural networks.* J. Pet. Sci. Eng., 197, doi: 10.1016/j.petrol.2020.107933.

Basu T., Dennis R., Al-Khobar B.D., Al Awadi W., Isby S.J., Vervest E. and Mukherjee R.; 2002: *Automated facies estimation from integration of core, petrophysical logs, and borehole images.* In: Proc. AAPG Search and Discovery, AAPG Annual Meeting, Houston, TX, USA, Article #90007.

Boser B.E., Guyon I.M. and Vapnik V.N.; 1992: *A training algorithm for optimal margin classifiers.* In: Haussler D. (ed), COLT92: 5th Annual Workshop on Computational Learning Theory, Pittsburgh, Pennsylvania, USA, 27-29 July 1992, Association for Computing Machinery, New York, NY, USA, pp. 144-152, doi: 10.1145/130385.130401.

Ceci M., Hollmén J., Todorovski L., Vens C. and Džeroski S. (eds); 2017: *Machine learning and knowledge discovery in databases*. European Conference, ECML PKDD 2017, Skopje, Macedonia, Part II, Springer Cham, Switzerland, 866 pp., doi: 10.1007/978-3-319-71246-8.

Chai H., Li N., Xiao C., Liu X., Li D., Wang C. and Wu D.; 2009: *Automatic discrimination of sedimentary facies and lithologies in reef-bank reservoirs using borehole image logs.* Appl. Geophys., 6, 17-29, doi: 10.1007/s11770-009-0011-4.

Chawshin K., Gonzalez A., Berg C.F., Varagnolo D., Heidari Z. and Lopez O.; 2021: *Classifying lithofacies from textural features in whole core CT-scan images*. SPE Reservoir Eval. Eng., 24, 341-357, doi: 10.2118/205354-PA.

Cover T. and Hart P.; 1967: *Nearest neighbor pattern classification.* IEEE Trans. Inf. Theory, 13, 21-27, doi: 10.1109/TIT.1967.1053964.

Dubois M.K., Bohling G.C. and Chakrabarti S.; 2007: *Comparison of four approaches to a rock facies classification problem.* Comput. Geosci., 33, 599-617, doi: 10.1016/j.cageo.2006.08.011.

Duchi J., Hazan E. and Singer Y.; 2011: *Adaptive subgradient methods for online learning and stochastic optimization.* J. Mach. Learn. Res., 12, 2121-2159, doi: 10.5555/1953048.2021068.

Esrafili-Dizaji B., Kiani Harchegani F., Rahimpour-Bonab H. and Kamali M.R.; 2013: *Controls on reservoir quality in the early Triassic Kangan Formation, Iran.* In: Pöppelreiter M. (ed), Permo-Triassic Sequence of the Arabian Plate, EAGE, 10, pp. 219-245, doi: 10.3997/9789462820074.

GISGeography; 2025: *Middle East map - political, physical, administrative.* <gisgeography.com/middle-east-map/#Administration-Map> (accessed May 2025).

Hall B.; 2016: *Facies classification using machine learning.* The Leading Edge, 35, 906-909, doi: 10.1190/tle35100906.

Hall J., Ponzi M., Gonfalini M. and Maletti G.; 1996: *Automatic extraction and characterisation of geological features and textures from borehole images and core photographs.* In: Proc. SPWLA 37th Annual Logging Symposium, New Orleans, LA, USA, Paper SPWLA-1996-CCC.

Hastie T., Tibshirani R. and Friedman J.; 2009: *The elements of statistical learning.* Springer, New York, NY, USA, 745 pp., doi: 10.1007/978-0-387-84858-7.

Imamordiev Y. and Sukhosta L.; 2019: *Lithological facies classification using deep convolutional neural network.* J. Pet. Sci. Eng., 174, 216-228, doi: 10.1016/j.petrol.2018.11.023.

Ioffe S. and Szegedy C.; 2015: *Batch normalization: accelerating deep network training by reducing internal covariate shift.* Proc. Machine Learning Res., 37, 448-456.

Kingma D.P. and Ba J.L.; 2014: *Adam: a method for stochastic optimization.* In: Proc. 3rd International Conference for Learning Representations, San Diego, CA, USA, arXiv 1412.6980, doi: 10.48550/arXiv.1412.6980.

Li J., Liu S., Zhang J., Fan Z., Sun Z., Zhang M., Yuan Y. and Zhang P.; 2015: *Architecture and facies model in a non-marine to shallow-marine setting with continuous base-level rise: an example from the Cretaceous Denglouku Formation in the Changling Depression, Songliao Basin, China.* Mar. Petrol. Geol., 68, 381-393, doi: 10.1016/j.marpetgeo.2015.09.002.

Li Y. and Anderson-Sprecher R.; 2006: *Facies identification from well logs: a comparison of discriminant analysis and naïve Bayes classifier.* J. Pet. Sci. Eng., 53, 149-157, doi: 10.1016/j.petrol.2006.06.001.

Linek M., Jungmann M., Berlage T., Pechnig R. and Clauser C.; 2007: *Rock classification based on resistivity patterns in electrical borehole wall images.* J. Geophys. Eng., 4, 171-183, doi: 10.1088/1742-2132/4/2/006.

Milad B. and Slatt R.; 2018: *Impact of lithofacies variations and structural changes on natural fracture distributions.* Interpretation, 6, T873-T887, doi: 10.1190/INT-2017-0138.1.

Moghanloo H.G., Riahi M.A. and Bagheri M.; 2018: *Application of simultaneous prestack inversion in reservoir facies identification.* J. Geophys. Eng., 15, 1376-1388, doi: 10.1088/1742-2140/aab249.

Newberry B.M., Hansen S.M. and Perrett T.T.; 2004: *A method for analyzing textural changes within clastic environments utilizing electrical borehole images.* Gulf Coast Ass. Geol. Soc. Trans., 54, <archives.datapages.com/data/gcags/data/054/054001/531.htm>.

Perotti C.R., Carruba S., Rinaldi M., Bertozzi G., Feltre L. and Rahimi M.; 2011: *The Qatar-South Fars arch development (Arabian Platform, Persian Gulf): insights from seismic interpretation and analogue modelling.* In: Schattner U. (ed), New Frontiers in Tectonic Research - At the Midst of Plate Convergence, IntechOpen, pp. 325-352, doi: 10.5772/20299.

Pollastro R.M., Persits F.M. and Steinshouer D.W.; 1999: *Map showing geology, hydrocarbon fields, and geologic provinces of Iran.* U.S. Geol. Surv., Open-File Report 97-470G, U.S. Geological Survey, Reston, VA, USA, doi: 10.3133/ofr97470G.

Prabowo U.N., Ferdiyan A., Raharjo S.A., Sehah S. and Candra A.D.; 2023: *Comparison of facies estimation using support vector machine (SVM) and K-nearest neighbor (KNN) algorithm based on well log data.* Aceh Int. J. Sci. Technol., 12, 246-253, doi: 10.13170/aijst.12.2.28428.

Rahimi A. and Riahi M.A.; 2022: *Reservoir facies classification based on random forest and geostatistics methods in an offshore oilfield.* J. Appl. Geophys., 8, 245-256, doi: 10.1016/j.petlm.2021.10.006.

Saggaf M.M. and Nebrija E.L.; 2003: *A fuzzy logic approach for the estimation of facies from wire-line logs.* AAPG Bull., 87, 1223-1240, doi: 10.1306/02260301019.

Zeiler M.D.; 2012: *ADADELTA: an adaptive learning rate method.* arXiv, doi: 10.48550/arXiv.1212.5701.

Corresponding author: Mohammad Ali Riahi
Institute of Geophysics, University of Tehran
North Kargar Ave., Tehran, Iran
Phone: +98 21 61118219 ; e-mail: mariahi@ut.ac.ir